Energy and Built Environment 6 (2025) 1142–1155

Contents lists available at ScienceDirect

Energy and Built Environment

journal homepage: http://www.keaipublishing.com/en/journals/energy-and-built-environment/

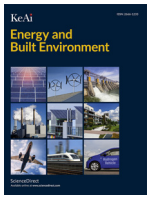

Full Length Article

Spatio-temporal analysis of LST, NDVI and SUHI in a coastal temperate city using local climate zone

Tania Sharmin [a,*], Adrian Chappell [b], Simon Lannon [a]

[a] Welsh School of Architecture, Cardiff University, Cardiff CF24 0DE, UK
[b] School of Earth and Environmental Sciences, Cardiff University, Cardiff CF24 0DE, UK

ARTICLE INFO

Keywords:
Urban morphology, Local climate zones (LCZs)
Land surface temperature (LST)
Normalised difference vegetation index (NDVI)
Urban heat island (SUHI)

ABSTRACT

Extreme heat due to changing climate poses a new challenge for temperate climates. The challenge is further aggravated by inadequate research, policy, or preparedness to effectively respond and recover from its impacts. While urban morphology is crucial in mitigating urban heat, it has received limited attention in urban planning, highlighting the need for further exploration, particularly in temperate regions. To illustrate the challenge and its potential mitigations, we use the example of the coastal temperate city of Cardiff. To establish the interrelations between urban morphology and urban heat island patterns, we explored the spatiotemporal variations in land surface temperature (LST), normalised difference vegetation index (NDVI), and surface urban heat island (SUHI) to local climate zone (LCZ) classification for Cardiff. Results showed a significant variation in SUHI in the LCZ zones. Both LST and NDVI land were found to vary significantly across the LCZ zones demonstrating their association with the urban form and morphology of the locality. For built-up areas, a more compact built-environment with smaller vegetation cover and larger building density was 2.0 °C warmer than the open built-environment when comparing the mean summer LSTs. On average, the natural classes exhibit a LST that is 8.0 °C lower than the compact built-environment and 6.0 °C lower than the open built-environment. Consequently, the high-density, built-up LCZs have a greater SUHI effect compared to the natural classes. Therefore, temperate climate cities will benefit from incorporating an open built-environment that has sufficient greenery and open spaces. These findings help determine the optimal urban form for temperate climates and develop heat mitigation strategies while planning, designing, or improving the new and existing urban areas. In addition, the LCZ map applied in this study for Cardiff will enable international comparison and testing of proven climate change adaptation and mitigation techniques for similar urban areas.

1. Introduction

As we approach a future of extended, hotter, and more frequent heat events, cities must intensify their efforts in planning for such extreme heat. The rising mortality risk attributable to ambient temperature rise across various cold and temperate climate cities [1,2], serves as a warning that extreme heat is a concern not only for tropical cities but also for those in temperate regions. The UK, generally considered to be part of a temperate region, is facing an unprecedented challenge posed by the high frequency of extreme heat. In the summer of 2022, the UK experienced record-breaking high temperatures, with certain areas exceeding 40 °C. This led the government to declare heat health warnings, signifying a national emergency for the first time [3]. While such temperature extremes are not rare, the high frequency of such occurrences is unprecedented. The rapid pace at which these changes have occurred has disrupted the healthcare system, transport infrastructure, and utility sectors, and caused economic losses at the local, regional, and national levels. Their study also highlighted that the UK is unprepared for upcoming extreme heat events, especially if they occur more frequently with the same intensity and duration, or if they are less frequent but more severe than the 2022 heatwaves. Current research on heat stress metrics, considering the combined effects of temperature, humidity, and urbanization, remains limited, as noted by [4,5]. Additionally, studies often neglect the role of climate and hydro meteorological variations in the context of urban heat stress, as highlighted by [6]. Therefore, there is a critical need to gain a deeper understanding of the mechanisms behind urban heat, particularly concerning the impacts of climate change and urbanization.

The impacts of extreme heat are further exacerbated by the surface urban heat island (SUHI) effect which is caused by the process of urbanization including changes in land use and land cover (LULC) and human behaviors. These phenomena lead to more days of intense heat on a local

* Corresponding author.
E-mail address: SharminT@Cardiff.ac.uk (T. Sharmin).

https://doi.org/10.1016/j.enbenv.2024.06.002
Received 9 April 2024; Received in revised form 29 May 2024; Accepted 10 June 2024
Available online 15 June 2024

level, linked with higher energy use for cooling in buildings and elevated human health risks due to heat. The SUHI intensity has significantly increased between 1990 and 2010, mainly due to urban expansion and the lack of green infrastructure in the city cores. Recent studies [7,8] indicate that this trend is expected to persist at least through 2030. Consequently, recognizing SUHI hotspot zones and adopting climate-driven planning measures is crucial to mitigate its effect.

There is an absence of evidence-backed urban planning policies aimed at enhancing urban thermal conditions in response to recent heat events in urban areas in general. This can be attributed to the lack of available data and a limited comprehension of how urban morphology influences the thermal conditions within the city. While weather data has become more available in recent years, the local or microclimate data remains scarce. As a result, our understanding of area or locality-specific climate change effects related to heat events is limited. Given the context, the local climate zone (LCZ) concept offers a novel perspective and methodology for investigating the urban heat island phenomenon, encouraging the integration of climate science research with policy planning efforts. The local climate zone framework developed by [9] serves as an verified classification system for land surfaces to identify the varying land surface types and to assess the impact of urban morphology on SUHI [10–12]. It can visually demonstrate the interplay between urban climatic conditions, surface structure, and land use and consequently, help identify the thermal environment management needs for various LCZs in cities [13]. The LCZ classification consists of 10 building and 7 land cover classes. The effectiveness of LCZ classification in depicting land surface characteristics and variations in microclimate is evident in literature ([13,14]). In this study we have used this framework to achieve the following objectives:

- Analyse the impact of urbanisation and urban morphology on local climate in a temperate city.
- Evaluate the effectiveness of local climate classification in explaining microclimate variations.
- Identify the top-performing and bottom-performing local climate zone (LCZ) categories in terms of their impacts on the local microclimate in the city.

To fulfil these goals, we employed the following approaches:

- Utilised a comprehensive LCZ map of the city.
- Explored the relationship between the LCZ classes and remote sensing data, including factors such as land surface temperature (LST), normalised difference vegetation index (NDVI), and the surface urban heat island (SUHI) effect.

In this study, we have used land surface temperature (LST) as it plays a vital role in describing microclimate conditions by representing the exchange of energy and matter between the surface of the earth and the lower layer of the atmosphere [15]. It serves as a valuable substitute for bridging information gaps and filling data voids in regions with limited weather station coverage [16]. The complete spectrum of thermal characteristics resulting from changes in LULC is not adequately captured by limited field measurements and isolated stationary networks [17,18]. Typically, LST is used to calculate surface temperature by leveraging indirect measurements of surface radiation, upward thermal radiance, and surface emissivity through thermal remote sensing techniques. Similar to LST, it is crucial for urban planning and policymakers to access greenspace data that is specific and available at a high spatial resolution [19]. Therefore, in this study, we apply normalised difference vegetation index (NDVI) which is a satellite-based measure of vegetation (abundance and health) to identify areas that suffer from a lack of green space. Simultaneously, comprehending the spatial pattern and structure of surface urban heat island (SUHI) is crucial for policymakers to develop localised mitigation action plans, target hot spots and allocate resources to respond to the adverse effect of SUHI [20]. This becomes especially important given the rising annual trends in SUHI observed in temperate climates [21].

2. Materials and methodology

Remote sensing tools have become indispensable for data collection and analysis across diverse fields. Key amongst these tools are Landsat, jointly operated by the United States Geological Survey (USGS) and NASA, MODIS (Moderate Resolution Imaging Spectroradiometer), a satellite sensor managed by NASA for observing Earth's surface and temperature, and Sentinel, an earth observation satellite operated by the European Space Agency (ESA). In a comprehensive systematic review to understand the impact of LULC on LST and outdoor thermal comfort, [22] found that Landsat was the most frequently employed tool in 57 % of studies, followed by MODIS at 12 %. Sentinel, operated by the European Space Agency (ESA), was less commonly used, accounting for only 3 % of studies. MODIS offers continuous images at a spatial resolution of 250–1000 m, allowing for regional and national-level analysis with daily data availability for short-term LULC changes. However, its broad area coverage may limit identifying specific land uses in smaller areas. MODIS provides a wide range of spectral bands, offering data on health, vegetation, atmospheric properties, and surface temperatures. Similarly, Sentinel also offers daily multispectral data collection, albeit limited to certain regions. In contrast, Landsat provides fine-resolution images up to 30 m, enabling detailed land cover analysis and historical data for LULC studies. However, it primarily collects visible and near-infrared spectral data, limiting its ability to provide comprehensive information on land use and surface temperature. Additionally, the revisit time of Landsat imagery is approximately 16 days, which may hinder the availability of daily data. Despite the limitations, using Landsat-8 images is an established way for estimation of LST and NDVI as demonstrated in various studies [23–29]. Additionally, it has been successfully applied in studies to investigate locations of different types of LCZ [30–32].

Consequently, in this study, we have applied satellite data for the recent years 2018, 2019, 2020, 2021 and 2022 for Cardiff during the summer months (June–August) to prepare LST, NDVI and SUHI maps and relate these to urban morphology of Cardiff by using GIS. This study focuses on the recent years and specifically the warmest months, which also coincide with the growing season in the UK, in response to the increased frequency of heat events in recent years. To promote sustainable urban development, we have conducted the first comprehensive city-wide assessment of LCZ mapping, comparing it with LST, NDVI, and SUHI data across the entire city. The data and accompanying map results will serve as a valuable resource for urban planners, designers, and policymakers, aiding in decision-making for planning and optimising climate-responsive designs.

2.1. Study area

The study focuses on Cardiff, the capital and largest city of Wales, located only 2.4 km from the sea. The city is encompassed by several water bodies, with the Taff and Rhymney rivers flowing in the east, the Bristol Channel to the south, the Severn Estuary to the southeast, and the river Ely to the west. The city is bordered by Vale of Glamorgan to the west and South Wales Valleys to the north, resulting in its growth being predominantly directed towards the eastern outskirts.

Cardiff experiences a temperate oceanic climate, classified as a 'Cfb' according to the Köppen climate classification [33]. Solar radiation levels are consistently high from March to October, with Cardiff experiencing an annual total solar radiation of 1337 kWh/m^2 and around 3029 hours of sunshine. The highest recorded annual dry bulb temperature is 24.7 °C, while the lowest is -4.8 °C [34].

According to data from the Office for National Statistics [35] the population size in Cardiff has increased by 4.7 %, from around 346,100 in 2011 to 362,400 in 2021. Approximately 41 % of the city's territory is set aside to protect its green spaces, while most of the brownfield land has already been developed [36]. In addition, there is a risk of flooding in areas like the river Taff and coastal plains, which constrains housing space due to tidal and river-related restrictions. According to the Organ-

Table 1
Remote sensing images used in the study.

LANDSAT_PRODUCT_ID	*row, path*	*Date image acquired*
LC08_L1TP_203,024_20,180,627_20,200,831_02_T1	24, 203	27–06–2018
LC08_L1TP_203,024_20,190,716_20,200,827_02_T1	24, 203	16–07–2019
LC08_L1TP_204,024_20,200,623_20,200,823_02_T1	24, 204	23–06–2020
LC08_L1TP_203,024_20,210,721_20,210,729_02_T1	24, 203	21–07–2021
LC08_L1TP_203,024_20,220,622_20,220,705_02_T1	24, 203	22–06–2022

isation for Economic Co-operation and Development [36], Cardiff needs to adopt more condensed urban development in order to meet the future housing demand. However, the impact of compact urban development on city's microclimate is unknown. Compounding the issue further, a geological study in Cardiff revealed that shallow groundwater temperatures beneath the city are 2 °C higher than the average groundwater temperature in the UK [37]. This additional warmth is attributed to the urban heat island (SUHI) effect. Consequently, in Cardiff, a spatial understanding of urban morphology and local SUHI conditions is vital for planning decisions aimed at mitigating the SUHI effect, highlighting the need for this study to inform future climate-proofing efforts.

2.2. Land surface temperature

Land surface temperature (LST) is essential for defining microclimate conditions, and it is readily available on a global scale through satellite imagery. The LST values were derived from Brightness Temperature (T_B) using the Semi-Automatic Classification Plugin in QGIS [38], applying the equation from [39]. As mentioned in the reference article [39], each of the LULC categories were assigned an emissivity value by reference to the emissivity classification scheme by [40].

$$S_t = \frac{T_B}{1 + \left(\lambda \times T_B/\rho\right) \ln \varepsilon} \tag{1}$$

where:

- S_t = The emissivity corrected LST
- λ = wavelength of emitted radiance (for which the peak response and the average of the limiting wavelengths ($\lambda = 11.5\ \mu m$) is used.
- $\rho = h \times c/\sigma\ (1.438 \times 10^{-2})$ m K
- h = Planck's constant = (6.626×10^{-34}) J s
- σ = Boltzmann constant = (1.38×10^{-23}) J/K
- c = velocity of light = (2.998×10^{8}) m/s
- ε = emissivity

Examining LST in relation to LCZ classification is a valuable approach to understanding differences amongst LCZ zones. Several studies have reported significant LST disparities across various LCZ classes, confirming LST's effectiveness in understanding the variation in urban form and surface properties [41,42]. In this study, five Landsat scenes from 2018 - 2022 were used, captured by Landsat Collection 2 Level 1, specifically Landsat 8 OLI/TIRS C2 L1. These scenes had a spatial resolution of 30 m and were obtained from the United States Geological Survey (USGS) Landsat Data Access Portal. The scenes were selected for the summer months between May- July, enabling the generation of LST and NDVI data. Scenes with minimal cloud cover (less than 15 %) were chosen to avoid misclassification caused by clouds and their shadows [42]. Additional information about these images can be found in Table 1. To compare with the LCZ, the image resolutions were adjusted to 100 m from the original 30 m. All spatial evaluations in this research were carried out using QGIS. Statistical examination of the gathered data was executed using the R Programming Tool.

2.3. Normalised difference vegetation index

Normalised difference vegetation index (NDVI) is a recognised method for quantifying vegetation by assessing the difference between near-infrared (NIR; Band 5) light (which vegetation strongly reflects) and Red light (Band 4 which vegetation absorbs) [43] (Eq. 2). Satellite instruments like Landsat have the necessary bands containing NIR and Red wavelengths.

$$NDVI = \frac{(NIR - Red)}{(NIR + Red)} \tag{2}$$

Typically, healthy vegetation (chlorophyll) reflects more near-infrared (NIR) and green light compared to other wavelengths, while absorbing more red and blue light. The NDVI always ranges from -1 to +1, but it does not establish distinct boundaries for different types of land cover. Negative values usually indicate the presence of water. Values near +1 suggest dense, healthy green leaves, and values near zero often mean a lack of green leaves. Smaller NDVI and reduced vegetation density may also indicate the impact of water deficiency on vegetation growth, thus revealing signs of drought. A change in NDVI for a pixel can result from altered plant health (spectral greenness) as well as changes in the number of plants and vegetation coverage (structure). However, NDVI cannot differentiate between spectral or structural changes. Alterations in land use and land cover (LULC) can significantly impact vegetation type and density [44]. Therefore, it's crucial to examine NDVI concerning LCZ classes to identify potential changes and effects. In this study, NDVI was computed using the Semi-Automatic Classification Plugin within QGIS [38] using Landsat data. The scenes were then resampled from 30 to 100 metres to align with the LCZ map.

2.4. Local climate zone (LCZ) and urban heat island (SUHI)

Understanding of the spatial distribution of SUHI intensity within LCZ categories remains limited in the UK, notably in Cardiff, especially during the recent prolonged periods of hot summer weather and frequent heat events. Therefore, a comprehensive understanding of how urban morphology affects the spatial distribution of SUHI in Cardiff is essential for effective climate planning and adaptation. The LCZ classification system has shown its effectiveness in measuring the urban heat island (SUHI) phenomenon [45]. In this research, we determine the SUHI across various LCZ categories by using LCZ-D (Low plants) as the benchmark for rural areas as also applied in [46]. The SUHI changes are calculated using the following equation [47]:

$$UHI = \frac{T_i - T_{mean}}{T_{sd}} \tag{3}$$

Here, T_i is the pixel value of LST, T_{mean} is the mean value of LST in LCZ-Dand T_{sd} is the standard deviation of LST within the study area.

The LCZ map of Cardiff has been extracted from the Global LCZ dataset developed by [48] based on the LCZ typology. A shape file for Cardiff is downloaded from the Digimap portal (https://digimap.edina.ac.uk/) to extract the region from the global data set. The data has a Coordinate Reference System of EPSG:4326 - WGS 84 which is exported to EPSG:32,630 - WGS 84 / UTM zone 30 N to match with the Landsat data.

2.5. Minimum detectable change (MDC)

This study applies the *minimum detectable change (MDC)* [49] to identify the differences in estimated means of the environmental properties such as LST, NDVI and SUHI. Our null hypothesis: $H_0 : \widehat{d}_{2,1} = 0$ posits

that there is no mean difference in environmental properties between various LCZ categories. The alternative hypothesis: H_1: $\hat{d}_{2,1} > 0$ suggests that the average difference in environmental properties varies between LCZ categories. The MDC, in this context, quantifies the uncertainty associated with making an incorrect conclusion and is linked to the probability of errors in drawing conclusions. The interpretation of the MDC is that it represents the smallest change in a measurement that can be confidently considered a real change, beyond the scope of measurement error, here with a 95 % level of confidence. In the case of a one-sided test, where $\hat{V}$ is an estimate of the spatial variance, MDC is calculated through the following equation:

$$\hat{d}_{2,1} = \mathrm{MDC} = \left(X_{1-\alpha} + X_{1-\beta}\right)\left(\frac{\hat{V}_1}{N_1} + \frac{\hat{V}_2}{N_1}\right)^{0.5} \quad (4)$$

Here, X is a standard normal distribution and N1 and N2 are the samples at each event. The α (the size of the significance test) and β represent probability of false rejection and probability of false acceptance, respectively. $1 - \beta$ is the power of the test.

3. Results

3.1. Local climate zones of Cardiff

The local climate zone (LCZ) of Cardiff is shown in Fig. 1. Approximately 54 % of the city consists of built-up areas (LCZ-1 to LCZ-6, LCZ-8, LCZ-10), while 38 % is covered by green spaces (LCZ-A to LCZ-D). The most dominant built-up LCZ class is LCZ-6 (Open lowrise) covering almost 40 % of the city (Fig. 1b). The next largest built-up LCZ classes include LCZ-8 (Large lowrise), LCZ-9 (Sparsely built) and LCZ-5 (Open midrise), respectively. Cardiff does not have any built-up areas in LCZ-7 (Lightweight lowrise) category which is a more prevalent category for cities in the developing countries. Also, Cardiff has a much lower population density and building density compared to many large cities in the west as can be seen in the lower number of built-up areas in the 'compact' category. Although it has some grid-cells in the LCZ-2 (Compact midrise) and LCZ-3 (Compact lowrise) categories, the number of grid-cells in the LCZ-1 (Compact highrise) category is very small covering only 0.1 % area of the city. The highrise buildings in Cardiff are mostly categorised as LCZ-4 (Open highrise). Cardiff also has some (1 %) heavy industrial areas categorised as LCZ-10 (Heavy industry). amongst the natural LCZ classes the prevailing category is LCZ-B (Scattered trees) covering 25 % of the area. The next main classes are LCZ-A (Dense trees) and LCZ-D (Low plants). There are no areas in LCZ-C (Bush, scrub) and LCZ-E (Bare rock or paved) categories and only a few grid cells in LCZ-F (Bare soil or sand) category. The percentage of water LCZ-G (Water) within the city landmass is around 1.3 %.

3.2. Spatio-temporal variation in land surface temperature in Cardiff

Fig. 2 shows the LST maps for Cardiff for the years 2018 to 2022. LSTs recorded during summer period ranges between 10.5 °C (2022) to 39.9 °C (2021). From the comparison of mean and median data, 2021 (mean summer LST of 30.5 °C) appears to be the warmest year with 2020 (mean summer LST of 24.9 °C) being the coolest. The LST data statistics for the years 2018, 2019, 2020, 2021 and 2022 is included in Table 2.

Table 2
LST data statistics for the years 2018, 2019, 2020, 2021 and 2022.

	LST_2018	LST_2019	LST_2020	LST_2021	LST_2022
Min.	20.3	14.5	16.4	22.8	10.5
1st Qu.	27.8	24.1	22.5	27.9	25.3
Median	30.4	26.9	24.7	30.5	28.0
Mean	30.1	26.5	24.9	30.5	28.0
3rd Qu.	32.6	28.9	27.3	33.1	30.8
Max.	39.1	35.2	36.1	39.9	39.2
NA's	195	7912	195	195	195

The change between the years does not follow a specific trend. It was not possible to find a cloud-free Landsat data for the summer period in 2019. The presented data for 2019 has cloud masking for a large region covering 7912 grid-cells with missing LST data. Therefore, the LST data for 2019 is excluded from further analysis.

Fig. 3 presents how the mean LST for the years 2018, 2020, 2021 and 2022 varies across the LCZ classes in Cardiff. Clearly the built-up LCZ classes have higher LSTs compared to the natural classes. The LST for the 'compact' areas are higher than the 'open' built-up areas. The 'compact' built-up classes have higher traffic flow, fewer tress or more impervious or paved surfaces compared to moderate/ lower traffic flow, abundant vegetation or plant cover and higher fraction of pervious surfaces in the 'open' built-up classes. The mean LST for the compact LCZ classes 1, 2 and 3 are 32.6 °C, 33.9 °C and 34.1 °C, respectively and the same for the open classes 4, 5 and 6 are 31.6 °C, 32.5 °C and 30.4 °C, respectively. The box-plot statistics for mean LST data (mean of 2018, 2020, 2021, 2022) for each LCZ classes can be found in Table 3.

On average, compact LCZ classes were 2.0 °C warmer than the open classes. amongst the built-up classes, LCZ-3 has the highest mean LST (34.1 °C) for higher building density and lower natural elements and LCZ-9 has the lowest (26.3 °C) due to a smaller number of buildings widely spaced across natural landscapes. Both LCZ-8 (30.8 °C) and LCZ-10 (31.8 °C) have lower mean temperatures compared to most 'compact' and 'open' built-up classes which is different from other cities such as São Paulo [50]. This means these classes in Cardiff may have a different physical character such as higher vegetation cover, lower paved surfaces etc. amongst the natural classes, LCZ-A has the lowest LST (23.7 °C) and LCZ-F has the highest LST (28.4 °C) due to their physical properties as also reported in the above study. On average, the natural classes exhibit a temperature that is 8.0 °C lower than the compact LCZ classes and 6.0 °C lower than the open LCZ classes.

To determine the statistical significance of the differences in estimated means, we applied the minimum detectable change (MDC) for LST, as shown in Table 4. It shows differences between various LCZ classes are statistically significant for most categories except between the following categories: LCZ-2 and LCZ-3, LCZ-1 and LCZ-5, LCZ-1 and LCZ-10, LCZ-4 and LCZ-10, LCZ-5 and LCZ-10, LCZ-9 and LCZ-B, LCZ-9 and LCZ-D and LCZ-B and LCZ-D.

3.3. Spatio-temporal variation in normalised difference vegetation index (NDVI)

The NDVI values for Cardiff (Fig. 4) are grouped into five categories: absence of vegetation (mainly water bodies, indicated by negative val-

Table 3
Box-plot statistics for mean LST data (mean of 2018, 2020, 2021, 2022) for each LCZ classes.

	1	2	3	4	5	6	8	9	10	A	B	D	F
Min	31.3	30.4	30.9	27.4	28.1	25.1	23.4	22.8	27.6	21.5	22.0	23.5	27.9
First Quartile	31.8	32.8	33.1	30.5	31.3	28.9	28.9	25.5	30.8	22.6	25.2	25.7	28.2
Median	32.6	33.9	34.1	31.6	32.5	30.4	30.8	26.3	31.8	23.7	26.3	26.4	28.4
Third Quartile	33.2	34.5	34.7	32.7	33.5	31.4	32.5	27.2	33.1	25.0	27.4	27.2	28.7
Maximum	34.5	36.5	35.9	35.8	35.5	35.1	37.4	29.9	36.5	28.5	30.6	29.4	28.8

Table 4
Minimum Detectable Change (MDC) for LST.

LCZ	1	2	3	4	5	6	8	9	10	A	B	D	F
1		1	1	1	0	1	1	1	0	1	1	1	1
2			0	1	1	1	1	1	1	1	1	1	1
3				1	1	1	1	1	1	1	1	1	1
4					1	1	1	1	0	1	1	1	1
5						1	1	1	0	1	1	1	1
6							1	1	1	1	1	1	1
8								1	1	1	1	1	1
9									1	1	0	0	1
10										1	1	1	1
11											1	1	1
12												0	1
14													1

ues), low vegetation (values ranging from 0.10 to 0.30), scattered vegetation (0.30 to 0.50), moderate to healthy vegetation (0.50 to 0.60), and dense vegetation (values exceeding 0.6). NDVI values in Cardiff varied from -0.06 to 0.64, with a mean NDVI of 0.32 during summer as calculated from the mean summer raster image indicating mostly scattered vegetation conditions across the city. Fig. 4 presents the NDVI values from 2018 to 2022, including the average NDVI for these years, showing minimal fluctuation in NDVI values over this period. They show that the north and northwest sections of the city are mainly characterised by scattered and moderate to healthy vegetation. In contrast, the central part has sparse vegetation, and the southern area along the estuary lacks almost any vegetation.

Fig. 5 illustrates NDVI variations across different LCZ classes during summer, highlighting significant differences in NDVI values amongst

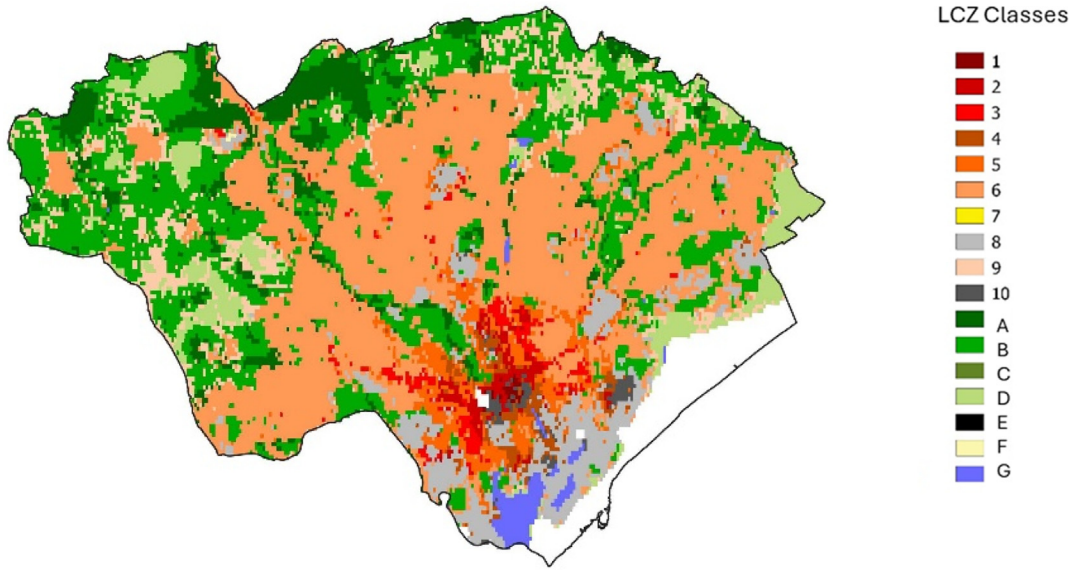

a.

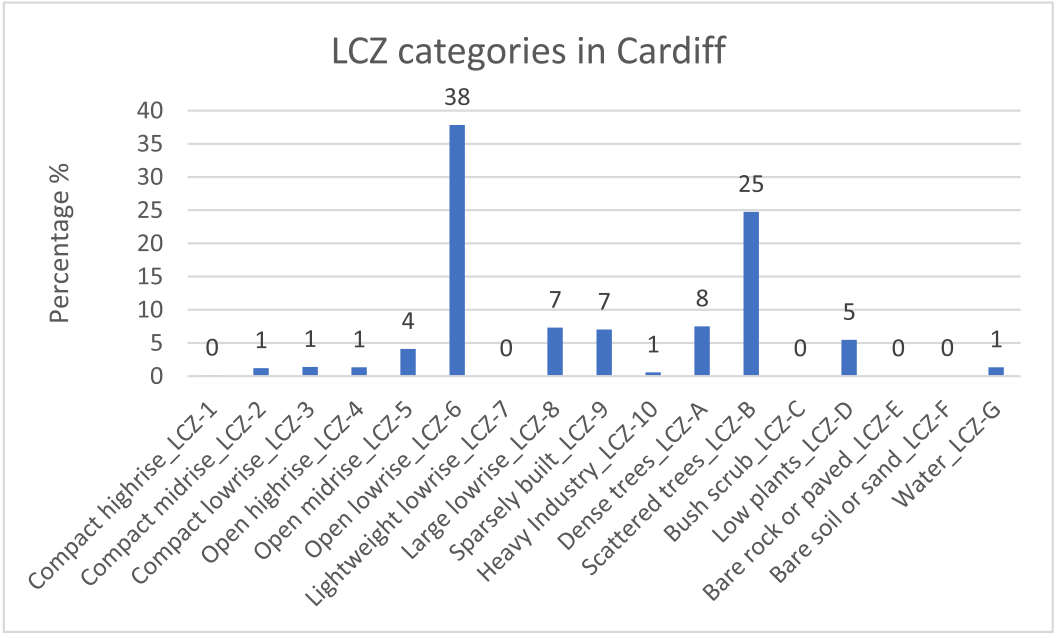

b.

Fig. 1. a. LCZ map of Cardiff, b. LCZ grid-cells in Cardiff, c. Google Map Images of common LCZ classes for Cardiff.

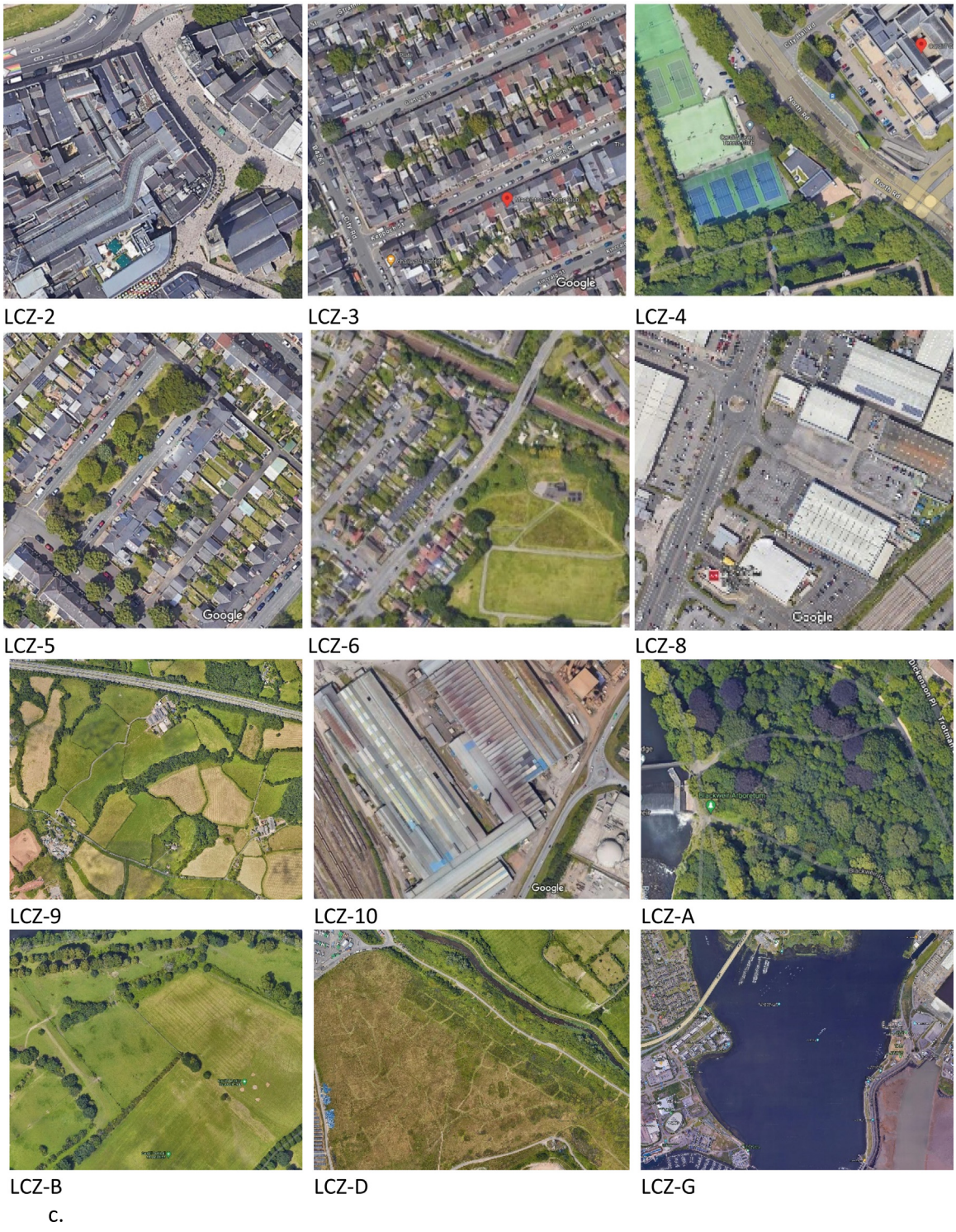

Fig. 1. Continued

the various LCZ categories. The built-up LCZ classes (LCZ-1 to LCZ-6) exhibit increasing median summer NDVI values of 0.07, 0.10, 0.11, 0.16, 0.17, and 0.26, respectively, as building density reduces and vegetation quantity increases. LCZ-9 has a higher median summer NDVI (0.46) compared to LCZ-1 (0.07) and LCZ-10 (0.06), which have minimal or no trees. Landcover classes LCZ-A, LCZ-B, and LCZ-D show a gradual decrease in median summer NDVI values of 0.50, 0.48, and 0.45, respectively, when compared to LCZ-F (0.08), which has few or no trees. The mean NDVI in compact LCZ areas is 0.10 lower than in open LCZ classes. Similarly, on average, natural LCZ classes display an NDVI 0.34 higher than built-up classes. The box-plot statistics (Table 5) show the mean NDVI data (mean of 2018, 2020, 2021, 2022) for each LCZ class.

The crosstabulation presenting the minimum detectable change (MDC) for NDVI (Table 6) shows the difference in mean is statistically significant in most cases, except between LCZ-1 and LCZ-2, LCZ-1 and LCZ-10, LCZ-1 and LCZ-F, LCZ-2 and LCZ-3, LCZ-4 and LCZ-8 and between LCZ-10 and LCZ-F in summer.

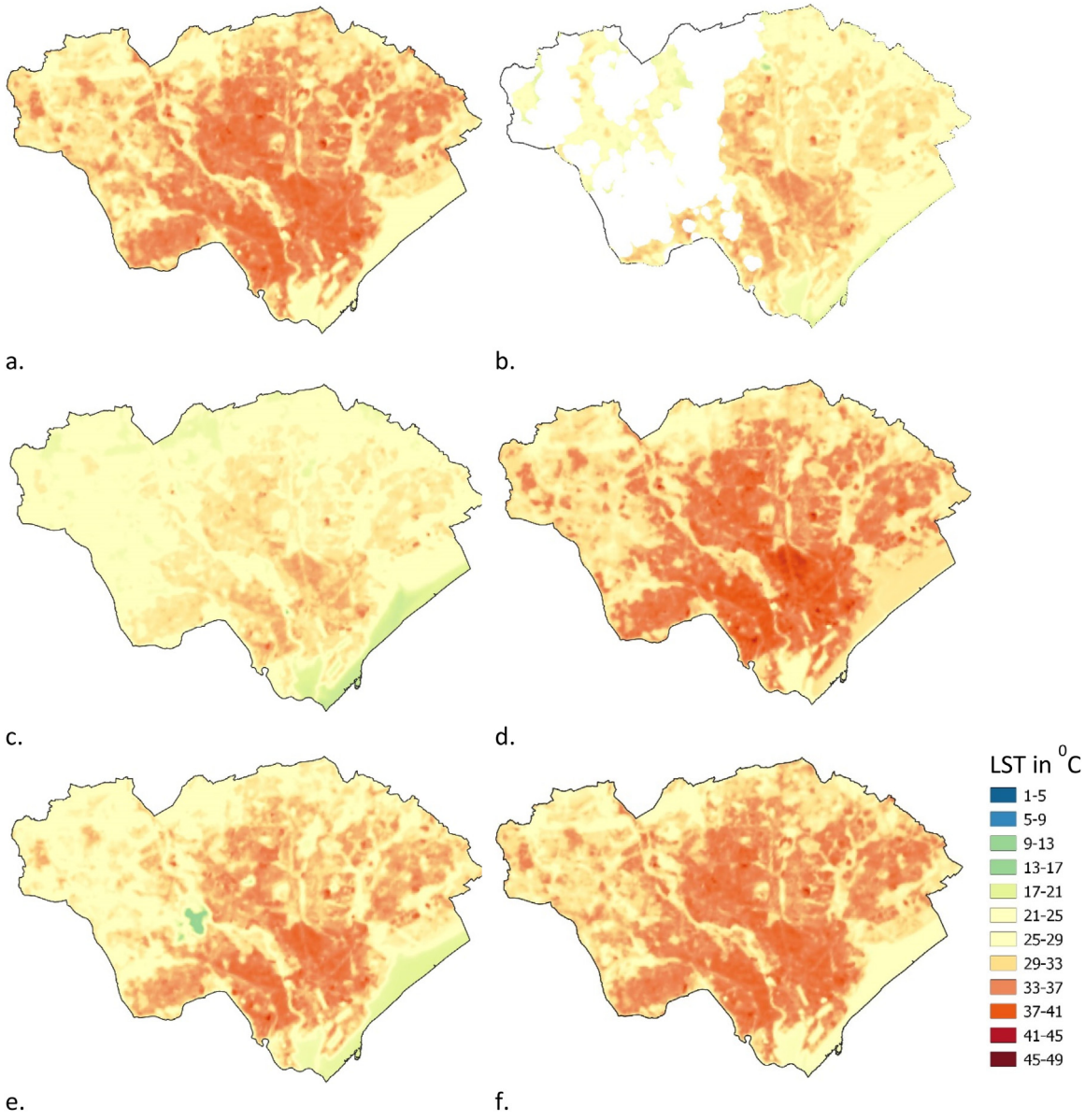

Fig. 2. Figures showing summer LST in a) 2018, b) 2019, c) 2020, d) 2021, e) 2022, and f) Mean LST of 2018, 2020, 2021 and 2022.

Table 5
Box-plot statistics for mean NDVI data (mean of 2018, 2020, 2021, 2022) for each LCZ classes.

	1	2	3	4	5	6	8	9	10	A	B	D	F
Min	-0.02	-0.02	0.02	-0.05	-0.01	-0.01	-0.06	0.21	-0.02	0.35	0.29	0.19	0.07
First Quartile	0.04	0.07	0.08	0.10	0.12	0.20	0.07	0.38	0.04	0.46	0.42	0.37	0.07
Median	0.07	0.10	0.11	0.16	0.17	0.26	0.13	0.46	0.06	0.50	0.48	0.45	0.08
Third Quartile	0.10	0.14	0.14	0.21	0.24	0.35	0.23	0.50	0.09	0.53	0.51	0.49	0.08
Maximum	0.19	0.24	0.23	0.36	0.41	0.56	0.46	0.61	0.15	0.62	0.64	0.62	0.08

3.4. Spatio-temporal variation in the surface urban heat island (SUHI)

Fig. 6 depicts the urban heat island (SUHI) during summers in Cardiff from 2018 to 2022 (excluding 2019 due to heavy cloud-cover), along with the mean SUHI for these years. The most noticeable SUHI effect occurred in 2018 and 2021. However, 2020 demonstrated a significantly reduced SUHI effect, likely due to the pandemic's influence as seen in LST patterns. The highest value of 4.4 °C was recorded in 2021, while the lowest was -5.2 °C in 2022. The SUHI effect is less prominent in the north and northwest city areas, where vegetation density or NDVI is higher. The central part exhibits a moderate SUHI effect, whereas the southern part experiences more substantial SUHI levels due to minimal vegetation. The SUHI is directly associated with building density and the presence of vegetation.

Fig. 7 displays the SUHI variation for different LCZ classes during the summer. Similar to the LST patterns, more high-density and compact built-up areas, such as LCZ-1 (Compact highrise), LCZ-2 (Compact midrise), and LCZ-3 (Compact lowrise), experience elevated SUHI. Across all landcover classes, except LCZ-F (Bare soil or sand) due to its material properties, SUHI values are lower. Within the built-up LCZ cat-

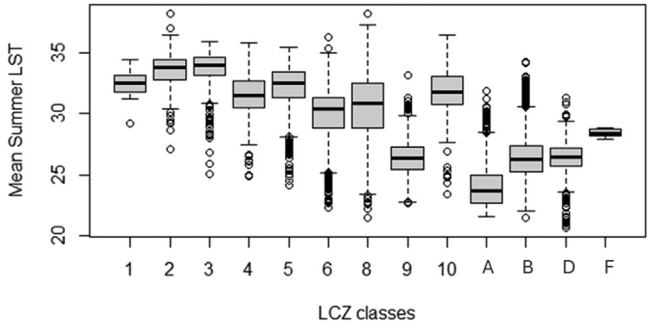

Fig. 3. Mean summer LST for different LCZ classes.

Table 6
Minimum Detectable Change (MDC) for NDVI.

LCZ	1	2	3	4	5	6	8	9	10	A	B	D	F
1		0	1	1	1	1	1	1	0	1	1	1	0
2			0	1	1	1	1	1	1	1	1	1	1
3				1	1	1	1	1	1	1	1	1	1
4					1	1	0	1	1	1	1	1	1
5						1	1	1	1	1	1	1	1
6							1	1	1	1	1	1	1
8								1	1	1	1	1	1
9									1	1	1	1	1
10										1	1	1	0
11											1	1	1
12												1	1
14													1

egories, LCZ-6 (Open lowrise) shows the lowest median SUHI of 1.3 °C, whereas LCZ 9 (Sparsely built) displays a negative median SUHI due to its natural surroundings (see Table 7). The most prominent SUHI is observed in LCZ-8 (Large lowrise) and LCZ-10 (Heavy industry) zones, where mean maximum values reach up to 3.6 °C and 3.3 °C, respectively. The box-plot statistics for mean SUHI data (mean of 2018, 2020, 2021, 2022) for each LCZ classes is presented in Fig. 7 and Table 7.

The minimum detectable change (MDC) for SUHI (Table 8) shows similar pattern to that of the MDC for LST. During summer, most LCZ categories are statistically different considering the SUHI. However, similar to LST, the absence of statistical differences is observed in the following classes: LCZ-2 and LCZ-3, LCZ-1 and LCZ-5, LCZ-1 and LCZ-10, LCZ-4 and LCZ-10, LCZ-5 and LCZ-10, LCZ-9 and LCZ-B, LCZ-9 and LCZ-D and LCZ-B and LCZ-D.

4. Discussion

4.1. LST characteristics in LCZ

The work showed that high-density and compact built-areas exhibit higher LST (Fig. 3), increased SUHI (Fig. 7) effect, and decreased NDVI (Fig. 5). Numerous studies have examined the differences in surface or air temperatures of LCZs, as indicated by references [14,51–58]. Studies in other coastal cities such as Hong Kong have also reported compact high-rise areas (LCZ-1) is most sensitive to extreme heat [59]. When

Table 8
Minimum Detectable Change (MDC) for SUHI.

LCZ	1	2	3	4	5	6	8	9	10	A	B	D	F
1		1	1	1	0	1	1	1	0	1	1	1	1
2			0	1	1	1	1	1	1	1	1	1	1
3				1	1	1	1	1	1	1	1	1	1
4					1	1	1	1	0	1	1	1	1
5						1	1	1	0	1	1	1	1
6							1	1	1	1	1	1	1
8								1	1	1	1	1	1
9									1	1	0	0	1
10										1	1	1	1
11											1	1	1
12												0	1
14													1

urban areas are densely constructed, the LST rises due to building materials and pavements absorbing solar radiation and storing it as heat. Additionally, the compact layout traps solar radiation within building masses, restricting its release into the night sky, resulting in the SUHI phenomenon. While the correlation between LST, NDVI and SUHI with LCZ classification is demonstrated in the above studies, the pattern and magnitude of the effect of the built environment for temperate climates were not fully explored.

The examination of annual LSTs between 2018–2022 reveals that global factors like pandemic may have played a role in lowering the LST in 2020 as also reported in a study conducted in Europe and North America [60]. Their study has also reported an increase in daytime LST during the pandemic over most parts of Europe due to a lesser reduction of solar radiation by atmospheric aerosols and water vapour content. This does not seem to be the case in Cardiff perhaps due to several surface-related factors such as large natural land coverage and proximity to the sea and lower population and building density compared to more high-density European cities. Cardiff also has a smaller fraction of 'compact' areas which are characterised by moderate to heavy traffic flow.

A significant portion of Cardiff built environment falls within the categories of LCZ-6 (Open low-rise). The mean difference in LST between compact and open urban zones is 2.0 °C during summer. The contrast is even more pronounced when compared to natural areas, with compact and open zones being respectively 8.0 °C and 6.0 °C warmer than these natural environments. This temperature disparity holds significant implications for urban climate, especially in the context of the growing frequency of heat events. Therefore, integrating open urban designs into the planning of both new and existing urban areas could considerably reduce LST, ultimately leading to an enhanced local microclimate.

This study's findings are consistent with previous research investigating differences in LST or air temperature within and between local climate zones (LCZs). For instance, [61] observed higher LST in compact residential areas compared to commercial areas in the city centre of Sendai, a typical Japanese metropolitan city. Similarly, in Kumasi city, Ghana, [62] noted a 1.2 °C increase in average surface temperature attributed to urbanisation effects. In Berlin, Germany, [63] documented average air temperature differences of approximately 1.0 °C (K) during

Table 7
Box-plot statistics for mean SUHI data (mean of 2018, 2020, 2021, 2022) for each LCZ classes.

LCZ_classes	1	2	3	4	5	6	8	9	10	A	B	F
Min	1.6	1.3	1.5	0.3	0.6	-0.4	-1.0	-1.2	0.4	-1.6	-1.5	0.5
First Quartile	1.8	2.1	2.2	1.3	1.6	0.8	0.8	-0.3	1.4	-1.3	-0.4	0.6
Median	2.0	2.4	2.5	1.7	2.0	1.3	1.4	-0.1	1.8	-0.9	-0.1	0.6
Third Quartile	2.2	2.6	2.7	2.0	2.3	1.6	2.0	0.3	2.2	-0.5	0.3	0.7
Maximum	2.6	3.3	3.1	3.1	3.0	2.8	3.6	1.1	3.3	0.7	1.4	0.8

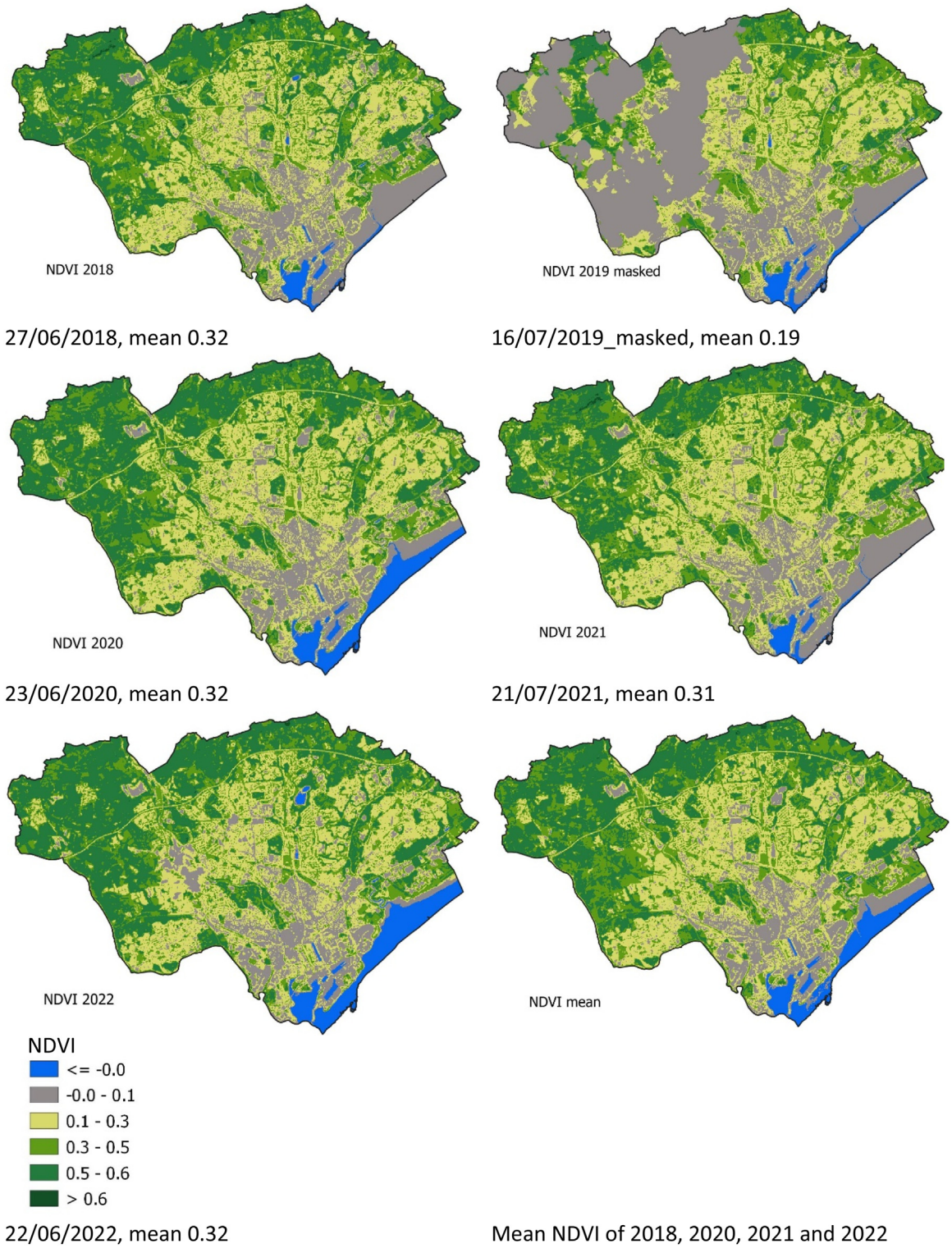

Fig. 4. Figures showing summer NDVI in 2018, 2019, 2020, 2021 and 2022.

summer nights between dense-trees (LCZ-A) and LCZ-6 (Open lowrise) areas.

In this study, it was observed that maximum LSTs in the categories of large low-rise buildings (LCZ-8) and heavy industrial buildings (LCZ-10) exceeded those observed in other compact built-classes (LCZ-1, 2, and 3). Several studies have previously documented the higher LSTs in industrial areas during daytime [64–66]. This phenomenon is attributed to the prevalence of impervious surfaces and extensive roof areas with low albedo, which aligns with findings from prior research [67,68]. These areas may benefit from additional vegetation to increase shading and reduce albedo on roof surfaces, thereby mitigating solar radiation in summer. A more comprehensive analysis, considering factors such as

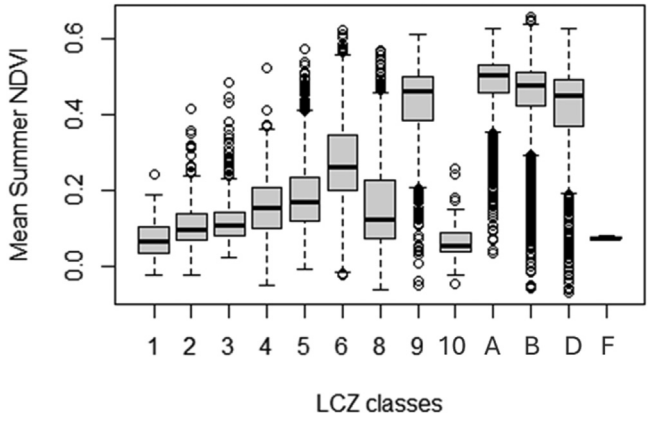

Fig. 5. Figures showing Mean Summer NDVI for various LCZ classes.

vegetation type, density, surface fraction, and thermal properties of pervious surfaces, is necessary to develop effective strategies for reducing LST in LCZ-8 and LCZ-10 [14].

Based on the analysis of the results, it becomes evident that LCZ-6 (Open lowrise) is the most suitable option for the urban climate of Cardiff. However, considering the potential for future population growth, it may not be feasible to expand the LCZ-6 further due to the scarcity of available buildable spaces. Conversely, proceeding with more intensified development is not recommended unless proper mitigation actions are implemented.

4.2. NDVI characteristics in LCZ

Numerous studies have explored the relationship between NDVI and LCZ classes. For example, [69]) conducted a study in three Chinese metropolises—Wuhan, Nanjing, and Shanghai—and discovered that NDVI had a significant mitigating effect on the heat risk index (HRI) in LCZ-1, LCZ-2, LCZ-4, and LCZ-5. Their recommendations for alleviating heat risk included transitioning compact LCZ types to open LCZ types, avoiding the configuration of LCZ-1 and LCZ-2, enhancing NDVI in existing LCZ-1, LCZ-2, LCZ-4, and LCZ-5 areas, increasing greenery by transforming mono-structures into composite structures with trees, shrubs, and grasses, and implementing greening of facades. Similarly, [70] in China found that NDVI had a notable cooling effect on the SUHI for most of the year. They found that NDVI performed best in terms of cooling within LCZ-F, particularly during summer and spring.

Concerning NDVI in Cardiff, the northern, northwestern, and northeastern regions of the city are abundantly covered by healthy vegetation, covering approximately 41 % of the city's land under its green space protection schemes. Nonetheless, the compact built areas in the southern part of the city exhibit a serious lack of vegetation, a concern that has been amplified by recent urban projects such as Roald Dahl Plass [71], which is nearly devoid of any significant greenery. The finding of our study shows that there is no difference in NDVI, between LCZ-1 and LCZ-2, LCZ-2 and LCZ-3, LCZ-1 and LCZ-10, LCZ-1 and LCZ-F, and between LCZ-10 and LCZ-F. This lack of differentiation can be attributed to the absence of vegetation and the prevalence of impervious land cover within these categories. But again, the lack of differences between the Open highrise (LCZ-4) and Large lowrise (LCZ-8) are not fully understood. It seems that LCZ has some limitations in distinguishing LCZ-8 and LCZ-10 from other categories.

4.3. SUHI characteristics in LCZ

The LCZ system has been extensively applied in research on SUHI [72]. Studies by [73] investigated LST characteristics across 18 LCZs in Beijing, revealing that compact and mid to low-rise built-up areas (LCZ-2, LCZ-3, LCZ-7, LCZ-8) tend to be the warmest zones, while water and vegetated types (LCZ-A, LCZ-B, LCZ-D, LCZ-G) are the coolest. SUHI events are most prevalent during summer and daytime conditions. LCZ-9 and LCZ-A, LCZ-B, LCZ-D, and LCZ-G show a seasonal pattern with smaller Annual Temperature Ranges (ATRs) due to factors such as leaf abscission and crop harvesting. Conversely, high-rise built-up zones (LCZ-1 and LCZ-4) experience higher ATRs because of seasonal variations in solar radiation. [74] examined the relationship between SUHI intensity and LCZ classes in Budapest, finding that as building density decreases, SUHI intensities also decrease. The highest intensities were observed in the city centre, while vegetated landcover LCZ classes exhibited the lowest SUHI intensities, sometimes resulting in cooling, as indicated by negative values.

Similar to LSTs, LCZ-8 (Large lowrise) and LCZ-10 (Heavy industry) zones in Cardiff showed the highest SUHI patterns. The substantial masses of large lowrise buildings capture solar radiation in thermal materials, and due to their dense urban layout, they struggle to release absorbed heat effectively, leading to SUHI effects. Similarly, heavy industrial structures release warm air, water vapour, CO2, and other harmful gases through the burning of fuels for heating and power, waste incineration, and industrial processes like metal milling and smelting which elevate urban temperatures. Studies by [46] reported Built-type LCZs had higher average SUHI-intensity than land-cover type LCZs in Dalian City, with the highest intensity (5.8 ˚C) observed in LCZ-10. In a similar study, [11] also reported significant SUHI variation amongst different LCZs, with higher SUHII observed in high-density built-up LCZs compared to open low-rise LCZs, reaching a maximum UHI mean of 5.3 ˚C.

4.4. LCZ-Application for Cardiff and its effectiveness

The study's findings from the Minimum Detectable Change (MDC) analysis highlight the effectiveness of LCZ classes in identifying microclimatic diversity. We have included MDC analysis for the first time in the field of urban climate research, to detect differences in the estimated means of environmental properties such as LST, NDVI, and SUHI. This approach is useful to represent the smallest change within the LCZ categories that can be confidently considered a real change, beyond the scope of measurement error, here with a 95 % level of confidence. We have identified statistically significant variations, particularly in summer, in LST, NDVI, and SUHI values within the LCZ categories.

In terms of LST, it is logical to observe no significant difference between LCZ-9 and LCZ-B, LCZ-9 and LCZ-D, and LCZ-B and LCZ-D. This is because these categories predominantly consist of impervious surfaces with minimal vegetation and scattered trees. Similarly, the lack of statistical difference between LCZ-2 and LCZ-3 as well as between LCZ-1 and LCZ-10, is understandable, as these categories are characterized by dense clusters of buildings and predominantly paved landscapes. However, the absence of differences in SUHI between the Open highrise (LCZ-4) and Open midrise (LCZ-5) categories compared to Heavy industry (LCZ-10) is not entirely clear.

Nonetheless, despite these limitations, while LCZ may not fully distinguish subtle differences in urban morphology, it remains suitable for categorising broader types such as compact and open built areas, as well as green and bare soil land cover. The LCZ method, with its integration of 3D landscape attributes, refined classification process, and identification of numerous landscape patches, has proven more effective than traditional LULC methods for classifying urban areas [75]. It proves to be a valuable tool for understanding distributions of LST, NDVI, and SUHI across cities and consequently, for guiding urban planning and design decisions aimed at improving their microclimates and mitigating climate impacts.

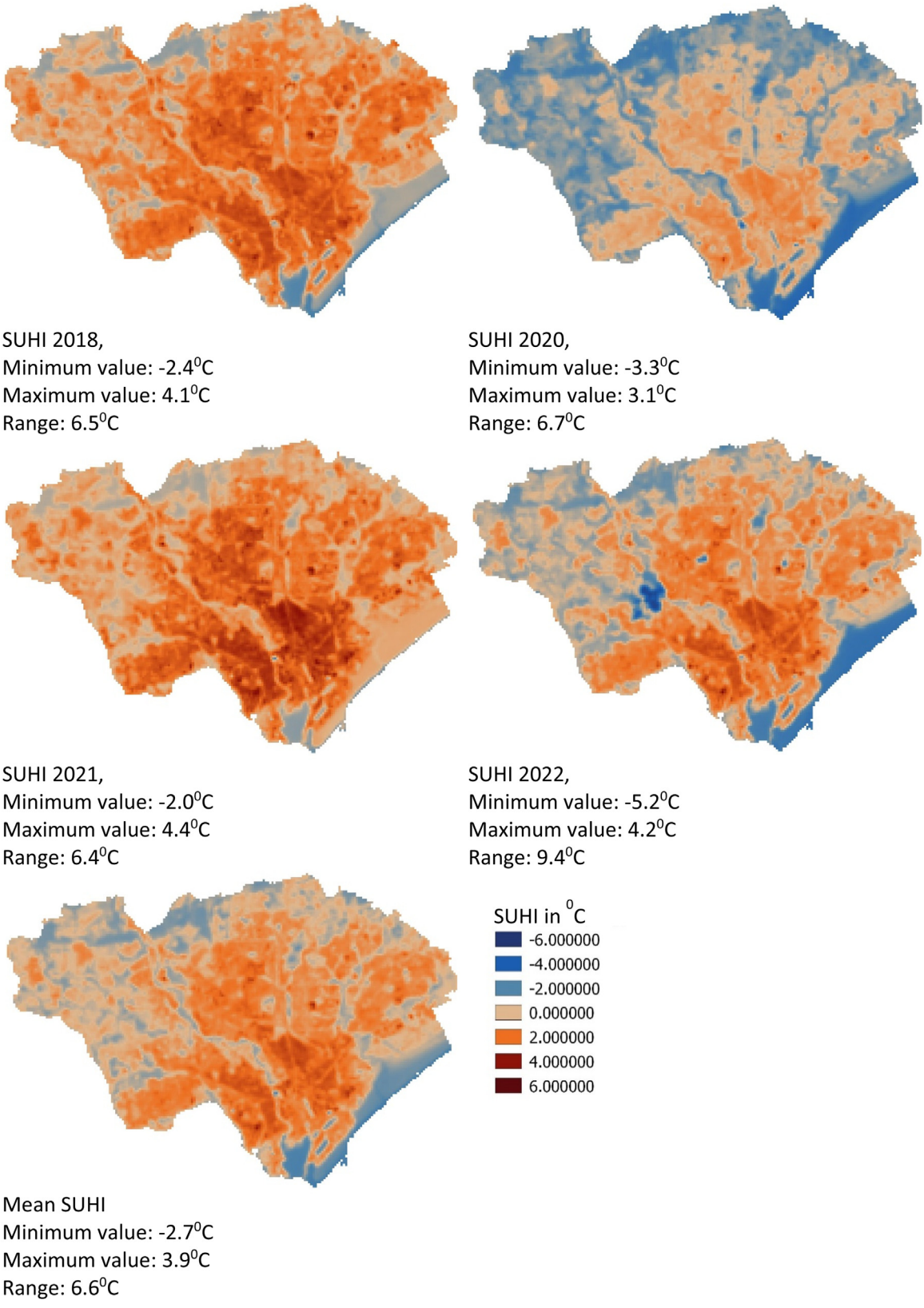

Fig. 6. Figures showing summer SUHI in 2018, 2019, 2020, 2021 and 2022.

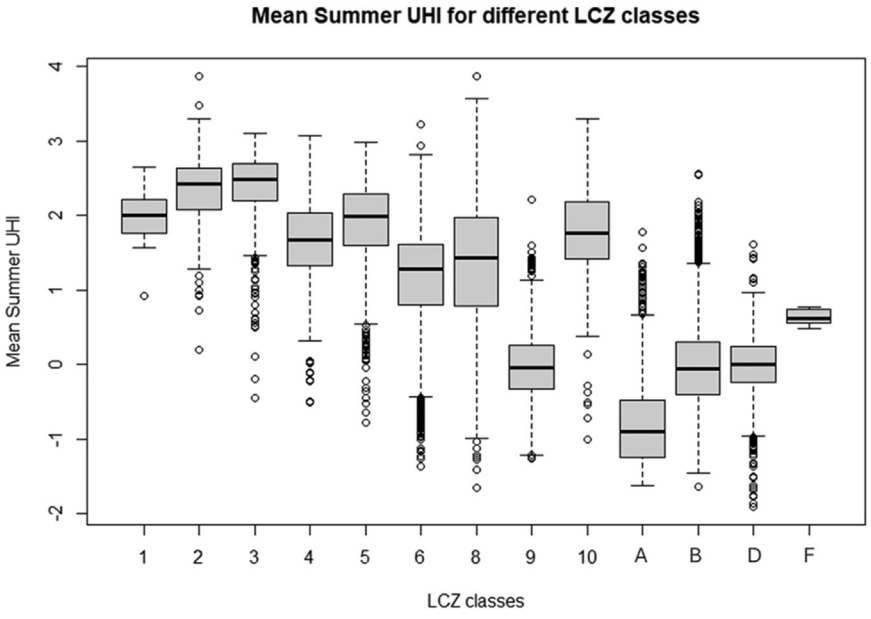

Fig. 7. Figures showing Mean Summer SUHI for various LCZ classes.

5. Conclusion

This study has explored the association between urban morphology through the application of LCZ map, LST, NDVI and SUHI effects, aiming to formulate an appropriate climate planning for Cardiff. This universally applicable description is crucial for supporting climate modelling and climate-sensitive urban planning policies. Specifically, the spatial patterns of LST, NDVI, and SUHI according to the LCZ categories play a vital role in comprehending the urban thermal environment. The key findings of this study are as follows: (1) The LCZ framework effectively categorises LST, NDVI, and SUHI observations in Cardiff, a temperate city. (2) Maps illustrating LST, NDVI, and SUHI changes from 2018 to 2022 reveal vital insights into differences across the city and hotspots. (3) The core results lie in LCZ-based variations of LST, NDVI, and SUHI, offering standardised spatial data for climate-conscious planning in Cardiff and cross-comparisons with LCZ-based studies in diverse climates. (4) Notably, open urban areas are cooler by 2.0 ˚C compared to compact urban regions. (5) On average, the natural classes exhibit a temperature that is 8.0 ˚C lower than the compact built-environment and 6.0 ˚C lower than the open built-environment. Given land constraints, an optimal urban planning strategy for Cardiff involves integrating high-density structures with ample green spaces and nature-based solutions to counter surface urban heat.

The findings of the study also demonstrate that vegetation cover can significantly affect the surface temperatures, aligning with similar research on the urban thermal environment. The observed inverse relationship between LST and NDVI underscores the importance of safeguarding the green spaces along the periphery of the city to mitigate the effects of extreme heat exposure. Hence, urban planners and policymakers should further emphasise on preserving the ecological roles of vegetation, wetlands, and water bodies, while devising strategies for built-up areas that coexist harmoniously with ecological conservation.

The research outcomes are crucial for understanding the impact of SUHI on densely populated areas in the event of frequent heatwaves. People in high-density areas are the most vulnerable to SUHI effect. Regardless of climate or wealth, unpreparedness can exacerbate SUHI consequences. The urban planners and policymakers should therefore consider the specific factors behind the SUHI effect in each LCZ classes to devise practical strategies for mitigation accordingly. These findings can help identify areas at risk of surface urban heating and aid in designing plans to lower LST, enhancing energy efficiency and thermal comfort in urban spaces.

To conclude, the outcomes of this research where the general public and local decision-makers are still unaware of the devastating effects of extreme heat events and SUHI. The study equips urban planners and designers with essential perspectives for appropriate urban planning and effective heat control. Particularly considering climate change challenges, these findings offer significant guidance for shaping future urbanisation trajectories. A limitation of this study is its focus on summer conditions when outdoor activities and heat-exposure risks are elevated. Further analysis during winter is needed, especially to understand the effect of SUHI.

Declaration of competing interest

The authors declare that they have no known competing financial interests or personal relationships that could have appeared to influence the work reported in this paper.

CRediT authorship contribution statement

Tania Sharmin: Writing – review & editing, Writing – original draft, Visualization, Validation, Software, Resources, Methodology, Investigation, Funding acquisition, Formal analysis, Data curation, Conceptualization. **Adrian Chappell:** Writing – review & editing. **Simon Lannon:** Writing – review & editing.

Acknowledgements

The time and resources dedicated for this work is funded by the Fung Global Fellowship Program at Princeton University. The author is grateful to Tsering Wangyal Shawa, Head of Princeton University Map and Geospatial Information center for providing necessary GIS training and support.

References

[1] A. Gasparrini, et al., Projections of temperature-related excess mortality under climate change scenarios, Lancet Planet. Heal. 1 (9) (2017) e360–e367, doi:10.1016/S2542-5196(17)30156-0.
[2] A. Gasparrini, Y. Guo, M. Hashizume, Mortalité attribuable au froid et à la chaleur : Analyse multi-pays, Environn., Risques et Sante 14 (6) (2015) 464–465, doi:10.1016/S0140-6736(14)62114-0.
[3] C. Howarth, A. Armstrong, N. Mcloughlin, and E. Murtagh, “Policy brief The 2022 heatwaves : England ’ s response and future preparedness for heat risk,” no. June, 2023.

[4] S.C. Sherwood and M. Huber, “An adaptability limit to climate change due to heat stress,” pp. 1–4, 2010, doi:10.1073/pnas.0913352107.
[5] K.W. Oleson, A. Monaghan, and O. Wilhelmi, “Interactions between urbanization, heat stress, and climate change,” pp. 525–541, 2015, doi:10.1007/s10584-013-0936-8.
[6] A. Hazem, J. Gil, M. Berghauser, Combining environmental and social dimensions in the typomorphological study of urban resilience to heat stress, Sustain. Cities Soc. 83 (April) (2022) 103971, doi:10.1016/j.scs.2022.103971.
[7] C. Shen, H. Hou, Y. Zheng, Y. Murayama, R. Wang, T. Hu, Prediction of the future urban heat island intensity and distribution based on landscape composition and configuration : A case study in Hangzhou, Sustain. Cities Soc. 83 (2318) (2022) 103992, doi:10.1016/j.scs.2022.103992.
[8] P. Tian, et al., Assessing spatiotemporal characteristics of urban heat islands from the perspective of an urban expansion and green infrastructure, Sustain. Cities Soc. 74 (August) (2021) 103208, doi:10.1016/j.scs.2021.103208.
[9] I.D. Stewart, T.R. Oke, Local climate zones for urban temperature studies, Bull. Am. Meteorol. Soc. 93 (12) (2012) 1879–1900, doi:10.1175/BAMS-D-11-00019.1.
[10] Y. Zheng, et al., Mapping the spatial distribution of nocturnal urban heat island based on Local Climate Zone framework, Build. Environ. 234 (November 2022) (2023) 110197, doi:10.1016/j.buildenv.2023.110197.
[11] G. Chen, Y. Chen, X. Tan, L. Zhao, Y. Cai, L. Li, Assessing the urban heat island effect of different local climate zones in Guangzhou, China, Build. Environ. 244 (June) (2023), doi:10.1016/j.buildenv.2023.110770.
[12] G. Chen, Y. Chen, H. He, J. Wang, L. Zhao, Y. Cai, Assessing the synergies between heat waves and urban heat islands of different local climate zones in Guangzhou, China, Build. Environ. 240 (March) (2023) 110434, doi:10.1016/j.buildenv.2023.110434.
[13] J. Yang, Y. Zhan, X. Xiao, J.C. Xia, W. Sun, X. Li, Investigating the diversity of land surface temperature characteristics in different scale cities based on local climate zones, Urban Clim. 34 (April) (2020) 100700, doi:10.1016/j.uclim.2020.100700.
[14] M. Unal Cilek, A. Cilek, Analyses of land surface temperature (LST) variability among local climate zones (LCZs) comparing Landsat-8 and ENVI-met model data, Sustain. Cities Soc. 69 (October 2020) (2021) 102877, doi:10.1016/j.scs.2021.102877.
[15] R. AZMI, C.S. TEKOUABOU KOUMETIO, E.B. DIOP, J. Chenal, Exploring the relationship between urban form and land surface temperature (LST) in a semi-arid region case study of Ben Guerir city - Morocco, Environ. Chall. 5 (April) (2021) 100229, doi:10.1016/j.envc.2021.100229.
[16] Y. joon Jeong, S. ik Lee, J. hyuk Lee, S.D. Jin, S.H. Son, W. Choi, Development of numerical land surface temperature model of Jeju Island, South Korea based on finite element method, Environ. Earth Sci. 80 (9) (2021) 1–12, doi:10.1007/s12665-021-09645-z.
[17] L. Hu, N.A. Brunsell, A new perspective to assess the urban heat island through remotely sensed atmospheric profiles, Remote Sens. Environ. 158 (2015) 393–406, doi:10.1016/j.rse.2014.10.022.
[18] H. Shen, L. Huang, L. Zhang, P. Wu, C. Zeng, Long-term and fine-scale satellite monitoring of the urban heat island effect by the fusion of multi-temporal and multi-sensor remote sensed data: A 26-year case study of the city of Wuhan in China, Remote Sens. Environ. 172 (2016) 109–125, doi:10.1016/j.rse.2015.11.005.
[19] J.D. Stowell, C. Ngo, M.P. Jimenez, P.L. Kinney, P. James, Development of a global urban greenness indicator dataset for 1,000+ cities, Data Br 48 (2023) 109140, doi:10.1016/j.dib.2023.109140.
[20] Y. Jamei, P. Rajagopalan, Q. (Chayn) Sun, Spatial structure of surface urban heat island and its relationship with vegetation and built-up areas in Melbourne, Australia, Sci. Total Environ. 659 (2019) 1335–1351, doi:10.1016/j.scitotenv.2018.12.308.
[21] N. Syahira, M. Harmay, M. Choi, The urban heat island and thermal heat stress correlate with climate dynamics and energy budget variations in multiple urban environments, Sustain. Cities Soc. 91 (January) (2023) 104422, doi:10.1016/j.scs.2023.104422.
[22] S. Patel, M. Indraganti, R.N. Jawarneh, A comprehensive systematic review: impact of land use/land cover (LULC) on land surface temperatures (LST) and outdoor thermal comfort, Build. Environ. 249 (August 2023) (2024) 111130, doi:10.1016/j.buildenv.2023.111130.
[23] C. Ru, et al., Land surface temperature retrieval from landsat 8 thermal infrared data over urban areas considering geometry effect: method and application, IEEE Trans. Geosci. Remote Sens. 60 (2022) 1–16, doi:10.1109/TGRS.2021.3088482.
[24] M. Lemus-Canovas, J. Martin-Vide, M.C. Moreno-Garcia, J.A. Lopez-Bustins, Estimating Barcelona’s metropolitan daytime hot and cold poles using Landsat-8 Land Surface Temperature, Sci. Total Environ. 699 (2020) 134307, doi:10.1016/j.scitotenv.2019.134307.
[25] C.B. Pande, et al., Predictive modeling of land surface temperature (LST) based on Landsat-8 satellite data and machine learning models for sustainable development, J. Clean. Prod. 444 (February) (2024) 141035, doi:10.1016/j.jclepro.2024.141035.
[26] D. Kumar, A. Soni, M. Kumar, Retrieval of land surface temperature from landsat-8 thermal infrared sensor data, J. Human, Earth, Futur. 3 (2) (2022) 159–168, doi:10.28991/HEF-2022-03-02-02.
[27] S. Guha, H. Govil, A. Dey, N. Gill, Analytical study of land surface temperature with NDVI and NDBI using Landsat 8 OLI and TIRS data in Florence and Naples city, Italy, Eur. J. Remote Sens. 51 (1) (2018) 667–678, doi:10.1080/22797254.2018.1474494.
[28] P.S. Kafer, S.B.A. Rolim, M.L. Iglesias, N.S. Da Rocha, L.R. Diaz, Land surface temperature retrieval by landsat 8 thermal band: Applications of laboratory and field measurements, IEEE J. Sel. Top. Appl. Earth Obs. Remote Sens. 12 (7) (2019) 2332–2341, doi:10.1109/JSTARS.2019.2913822.
[29] S.A. Ali, F. Parvin, A. Ahmad, Retrieval of land surface temperature from landsat 8 OLI and TIRS: A comparative analysis between radiative transfer equation-based method and split-window algorithm, Remote Sens. Earth Syst. Sci. 6 (1–2) (2023) 1–21, doi:10.1007/s41976-022-00079-0.
[30] M. Vaidya, R. Keskar, R. Kotharkar, Classifying heterogeneous urban form into local climate zones using supervised learning and greedy clustering incorporating Landsat dataset, Urban. Clim. 53 (November 2023) (2024) 101770, doi:10.1016/j.uclim.2023.101770.
[31] Y. Xu, C. Ren, M. Cai, N.Y.Y. Edward, T. Wu, Classification of local climate zones using aSTER and Landsat data for high-density cities, IEEE J. Sel. Top. Appl. Earth Obs. Remote Sens. 10 (7) (2017) 3397–3405, doi:10.1109/JSTARS.2017.2683484.
[32] G. Xu, X. Zhu, N. Tapper, B. Bechtel, Urban climate zone classification using convolutional neural network and ground-level images, Prog. Phys. Geogr. 43 (3) (2019) 410–424, doi:10.1177/0309133319837711.
[33] N. Rotas, R. Fotopoulou, M. Drosatos, P. Rakopoulos, D. Nikolopoulos, Adaptive dynamic building envelopes with solar power components: annual performance assessment for two pilot sites, Energies 16 (2023), doi:10.3390/en16052148.
[34] L. Wang, J. Gwilliam, P. Jones, Case study of zero energy house design in UK, Energy Build. 41 (11) (2009) 1215–1222, doi:10.1016/j.enbuild.2009.07.001.
[35] Office for National Statistics, “Census 2021,” Www.Ons.Gov.Uk/Census. [Online]. Available: https://www.ons.gov.uk/visualisations/censuspopulationchange/W06000015/
[36] Organisation for Economic Co-operation and Development, “Resilient cities - Cardiff.” [Online]. Available: https://www.oecd.org/cfe/regionaldevelopment/resilient-cities-cardiff.pdf
[37] G.J. Farr, A.M. Patton, D.P. Boon, D.R. James, B. Williams, D.I. Schofield, Mapping shallow urban groundwater temperatures, a case study from Cardiff, UK, Q. J. Eng. Geol. Hydrogeol. 50 (2) (2017) 187–198, doi:10.1144/qjegh2016-058.
[38] L. Congedo, Semi-automatic classification plugin documentation 5.0.0.1 Luca Congedo, 2016 [Online]. Available https://media.readthedocs.org/pdf/semiautomaticclassificationmanual-v5-fa/latest/semiautomaticclassificationmanual-v5-fa.pdf .
[39] Q. Weng, D. Lu, J. Schubring, Estimation of land surface temperature-vegetation abundance relationship for urban heat island studies, Remote Sens. Environ. 89 (4) (2004) 467–483, doi:10.1016/j.rse.2003.11.005.
[40] W.C. Snyder, Z. Wan, Y. Zhang, Y.Z. Feng, Classification-based emissivity for land surface temperature measurement from space, Int. J. Remote Sens. 19 (14) (1998) 2753–2774, doi:10.1080/014311698214497.
[41] J. Geletič, M. Lehnert, P. Dobrovolný, Land surface temperature differences within local climate zones, Based on two central European cities, Remote Sens 8 (10) (2016) 1–18, doi:10.3390/rs8100788.
[42] M. Cai, C. Ren, Y. Xu, K.K.L. Lau, R. Wang, Investigating the relationship between local climate zone and land surface temperature using an improved WUDAPT methodology – A case study of Yangtze River Delta, China, Urban. Clim. 24 (2018) 485–502, doi:10.1016/j.uclim.2017.05.010.
[43] GISGeography, “What is NDVI (normalized difference vegetation index)?” [Online]. Available: https://gisgeography.com/ndvi-normalized-difference-vegetation-index/
[44] J. Tan, D. Yu, Q. Li, X. Tan, W. Zhou, Spatial relationship between land-use/land-cover change and land surface temperature in the Dongting Lake area, China, Sci. Rep. 10 (1) (2020) 1–9, doi:10.1038/s41598-020-66168-6.
[45] B. Han, Z. Luo, Y. Liu, T. Zhang, L. Yang, Using Local Climate Zones to investigate Spatio-temporal evolution of thermal environment at the urban regional level: A case study in Xi’an, China, Sustain. Cities Soc. 76 (July 2021) (2022) 103495, doi:10.1016/j.scs.2021.103495.
[46] Z. Shi, J. Yang, Y. Zhang, X. Xiao, J.C. Xia, Urban ventilation corridors and spatiotemporal divergence patterns of urban heat island intensity: a local climate zone perspective, Environ. Sci. Pollut. Res. 29 (49) (2022) 74394–74406, doi:10.1007/s11356-022-21037-9.
[47] M.N. Rahman, et al., Impact of urbanization on urban heat island intensity in major districts of bangladesh using remote sensing and geo-spatial tools, Climate 10 (1) (2022), doi:10.3390/cli10010003.
[48] M. Demuzere, et al., A global map of local climate zones to support earth system modelling and urban-scale environmental science, Earth Syst. Sci. Data 14 (8) (2022) 3835–3873, doi:10.5194/essd-14-3835-2022.
[49] N.P. Webb, et al., Reducing sampling uncertainty in aeolian research to improve change detection, J. Geophys. Res. Earth Surf. 124 (6) (2019) 1366–1377, doi:10.1029/2019JF005042.
[50] L.S. Ferreira, D.H.S. Duarte, Exploring the relationship between urban form, land surface temperature and vegetation indices in a subtropical megacity, Urban. Clim. 27 (November 2018) (2019) 105–123, doi:10.1016/j.uclim.2018.11.002.
[51] P. Du, J. Chen, X. Bai, W. Han, Urban Climate Understanding the seasonal variations of land surface temperature in Nanjing urban area based on local climate zone, Urban Clim. 33 (November 2019) (2020) 100657, doi:10.1016/j.uclim.2020.100657.
[52] D. Fenner, F. Meier, B. Bechtel, M. Otto, and D. Scherer, “Intra and inter ‘ local climate zone ’ variability of air temperature as observed by crowdsourced citizen weather stations in Berlin, Germany,” vol. 26, no. 5, pp. 525–547, 2017, doi:10.1127/metz/2017/0861.
[53] J. Geletič and M. Lehnert, “GIS-based delineation of local climate zones : The case of medium-sized Central European cities,” vol. 23, no. 4, pp. 2–12, 2016, doi:10.1515/mgr-2016-0012.
[54] S. Jiang, et al., Surface air temperature differences of intra- and inter-local climate zones across diverse timescales and climates, Build. Environ. 222 (163) (2022) 109396, doi:10.1016/j.buildenv.2022.109396.
[55] N. Li, J. Yang, Z. Qiao, and Y. Wang, “Urban thermal characteristics of local climate zones and their mitigation measures across cities in different climate zones of China,” 2021.
[56] Y. Chen, B. Zheng, and Y. Hu, “Mapping local climate zones using ArcGIS-based method and exploring land surface temperature characteristics in Chenzhou, China,” 2020.

[57] C. Res, P. Dobrovolný, M. Jurek, M. Lehnert, and J. Geletic, "Temperature differences among local climate zones established by mobile measurements in two central European cities," vol. 75, pp. 53–64, 2018.
[58] F. Meier, D. Fenner, T. Grassmann, M. Otto, D. Scherer, Urban Climate Crowdsourcing air temperature from citizen weather stations for urban climate research, Urban. Clim. 19 (2017) 170–191, doi:10.1016/j.uclim.2017.01.006.
[59] R. Du, C.H. Liu, X. Li, C.Y. Lin, Interaction among local flows, UHI, coastal winds, and complex terrain: Effect on urban-scale temperature and building energy consumption during heatwaves, Energy Build. 303 (September 2023) (2024) 113763, doi:10.1016/j.enbuild.2023.113763.
[60] B.R. Parida, S. Bar, D. Kaskaoutis, A.C. Pandey, S.D. Polade, S. Goswami, Impact of COVID-19 induced lockdown on land surface temperature, aerosol, and urban heat in Europe and North America, Sustain. Cities Soc. 75 (September) (2021) 103336, doi:10.1016/j.scs.2021.103336.
[61] X. Zhou, T. Okaze, C. Ren, M. Cai, Y. Ishida, H. Watanabe, Evaluation of urban heat islands using local climate zones and the influence of sea-land breeze, Sustain. Cities Soc. 55 (October 2019) (2020) 102060, doi:10.1016/j.scs.2020.102060.
[62] C. Mensah, et al., Impact of urban land cover change on the garden city status and land surface temperature of Kumasi Impact of urban land cover change on the garden city status and land surface temperature of Kumasi, Cogent Environ. Sci. 6 (1) (2020), doi:10.1080/23311843.2020.1787738.
[63] D. Fenner, F. Meier, D. Scherer, A. Polze, Urban Climate Spatial and temporal air temperature variability in Berlin, Germany, during the years 2001 –2010, Urban. Clim. 10 (2014) 308–331, doi:10.1016/j.uclim.2014.02.004.
[64] Y.Y. Li, H. Zhang, W. Kainz, Monitoring patterns of urban heat islands of the fast-growing Shanghai metropolis, China: using time-series of landsat TM/ETM+ data, Int. J. Appl. Earth Obs. Geoinf. 19 (1) (2012) 127–138, doi:10.1016/j.jag.2012.05.001.
[65] I.D. Stewart, T.R. Oke, E.S. Krayenhoff, Evaluation of the 'local climate zone' scheme using temperature observations and model simulations, Int. J. Climatol. 34 (4) (2014) 1062–1080, doi:10.1002/joc.3746.
[66] A. Buyantuyev, J. Wu, Urban heat islands and landscape heterogeneity: Linking spatiotemporal variations in surface temperatures to land-cover and socioeconomic patterns, Landsc. Ecol. 25 (1) (2010) 17–33, doi:10.1007/s10980-009-9402-4.
[67] E. Matsaba, E. Fakharizadehshirazi, A. Ochieng, J. Bosco, J. Mwibanda, S. Sodoudi, Urban climate inter-local climate zone di ff erentiation of land surface temperatures for management of urban heat in Nairobi City, Kenya, Urban. Clim. 31 (September 2019) (2020) 100540, doi:10.1016/j.uclim.2019.100540.
[68] J. Geleti˘, M. Lehnert, P. Dobrovolný, Land surface temperature differences within local climate zones, based on two central European cities, Remote Sens. (2016) 1–18, doi:10.3390/rs8100788.
[69] Y. Xiang, C. Yuan, Q. Cen, C. Huang, and C. Wu, "Heat risk assessment and response to green infrastructure based on local climate zones," vol. 248, no. November 2023, 2024.
[70] Y. Luo, J. Yang, Q. Shi, Y. Xu, M. Menenti, M.S. Wong, Seasonal cooling effect of vegetation and albedo applied to the LCZ classification of three Chinese megacities, Remote Sens 15 (23) (2023), doi:10.3390/rs15235478.
[71] S. Lehmann, Urban regeneration: a manifesto for transforming UK cities in the age of climate change, 2019, doi:10.1007/978-3-030-04711-5.
[72] B. Bechtel, et al., Urban climate SUHI analysis using local climate zones — a comparison of 50 cities, Urban. Clim. 28 (January) (2019) 100451, doi:10.1016/j.uclim.2019.01.005.
[73] J. Quan, "Multi-temporal effects of urban forms and functions on urban heat islands based on local climate zone classification," pp. 9–11, 2019.
[74] C. Dian, R. Pongrácz, Z. Dezső, J. Bartholy, Urban Climate Annual and monthly analysis of surface urban heat island intensity with respect to the local climate zones in Budapest, Urban. Clim. 31 (December 2019) (2020) 100573, doi:10.1016/j.uclim.2019.100573.
[75] R. Jiang, C. Xie, Z. Man, A. Afshari, S. Che, LCZ method is more effective than traditional LUCC method in interpreting the relationship between urban landscape and atmospheric particles, Sci. Total Environ. 869 (January) (2023) 161677, doi:10.1016/j.scitotenv.2023.161677.